RESEARCH NOTE

Finite Element Analysis of Buckling of Thin Cylindrical Shell Subjected to Uniform External Pressure

B. Prabu[*], N. Rathinam, R. Srinivasan, K.A.S. Naarayen

Department of Mechanical Engineering, Pondicherry Engineering College, Pondicherry-605014, India

ABSTRACT
One of the common failure modes of thin cylindrical shell subjected external pressure is buckling. The buckling pressure of these shell structures are dominantly affected by the geometrical imperfections present in the cylindrical shell which are very difficult to alleviate during manufacturing process. In this work, only three types of geometrical imperfection patterns are considered namely (a) eigen affine mode imperfection pattern, (b) inward half lobe axisymmetric imperfection pattern extended throughout the height of the cylindrical shell and (c) local geometrical imperfection patterns such as inward dimple with varying wave lengths located at the mid-height of the cylindrical shell. ANSYS FE non-linear buckling analysis including both material and geometrical non-linearities is used to determine the critical buckling pressure. From the analysis it is found that when the maximum amplitude of imperfections is $1t$, the eigen affine imperfection pattern gives out the lowest critical buckling pressure when compared to the other imperfection patterns considered. When the amplitude of imperfections is above $1t$, the inner half lobe axisymmetric imperfection pattern gives out the lowest critical buckling pressure when compared to the other imperfection patterns considered.

© 2009 JSM. All rights reserved

1 INTRODUCTION

THIN cylindrical shells have wide applications in marine, nuclear, mechanical, and civil and space structures which are highly susceptible for imperfections and they have efficient load carrying capacity with weight economy. Generally these thin cylindrical shells fail by buckling under external pressure. Hence the design of thin cylindrical shells under external pressure should be based on buckling criteria. Buckling phenomena occurs when most of the strain energy which is stored as membrane energy can be converted to bending energy requiring large deformation resulting in catastrophic failure. If thin cylindrical shell is not ring stiffened, its buckling resistance is very poor and they fail by non-symmetric bifurcation buckling. One method of greatly improving the buckling resistance of such long thin cylindrical shell is to ring stiffen them in their flanges. If, however, the ring stiffeners are not strong enough, the ring-shell combination can collapse due to application of uniform external pressure. Such mode of failure is known as general instability [1, 2]. If the ring stiffeners are strong enough, the bare shell in-between the ring stiffeners will collapse which is called as local collapse [3].

The imperfections which cause failure in thin cylindrical shells are grouped into three major groups and they are, geometrical (for example, out-of-straightness, initial ovality, and geometrical eccentricities, dents, swells, circularity, cylindricity etc.), structural (residual stresses and material inhomogenities), and loading imperfections (non-uniform edge load distribution, unintended edge moments, load eccentricities, and load misalignments as well

_____

[*] Corresponding author. Tel: +91 960 099 4737, +91 900 353 1631.
  E-mail address: rathinam_pec@yahoo.in.

as imperfect boundary conditions). Also the constructional defects, such as small holes, cut outs, rigid inclusions, and delaminations could be counted as structural imperfections. Out of all these imperfections, the geometrical imperfections are more dominant in determining the load carrying capacity of thin cylindrical shells.

2   LITERATURE REVIEW

The stability of circular cylindrical shells under external pressure has been widely investigated. The classical elastic buckling theory predicts the bifurcation buckling pressure of perfect thin cylindrical shell without stiffeners under uniform external pressure is given in Timoshenko and Gere [4] and analytical solution based on Donnell stability equation in uncoupled form is given in Brush and Almorth [5]. Bushnell [6] reported both analytical and numerical efforts and experimental investigations carried out before 1985. It was reported that both analytical results and experimental results are widely deviating. It was also reported that the cause for this deviation is due to inevitable differences called imperfections present in the real structure from the perfect structure. Out of all other imperfections, geometrical imperfections sensitively affect the buckling behaviour of cylindrical shell under external pressure [3]. There were many numerical and analytical studies, investigating the strength of the cylinders with specific imperfection forms. For example, Teng and Song [7], Featherston [8], Kim and Kim [9], and khelil [10], in their work had taken the first eigen mode shape obtained from linear buckling analysis as imperfection shape and studied the buckling behaviour of thin shell structures. Similarly for example, Pircher et al. [11], Koiter [12], Khamlichi et al. [13], and Schiender [14] had taken axisymmetric imperfection pattern extended over the entire length of the cylindrical shell and studied the buckling behaviour of the shell structure. And for example, Hutchinson et al. [15], Amazigo and Budiansky [16], Shen and Li [17], and Schiender and Brede [3] had taken local geometrical imperfection pattern called dimple and studied the buckling behavior of shell structure. Hence in this numerical work, efforts are made to determine whether distributed geometrical imperfections or local geometrical imperfections dominantly affects the buckling strength of local collapse of bare thin cylindrical shell portion between stiffeners under external pressure. The following imperfection patterns only are taken for study namely a) first eigen mode shape, b) inward half lobe axisymmetric imperfection pattern extended over the entire length of the cylindrical shell and c) inward axisymmetric dimple located at the mid-height of the cylindrical shell with varying wave length (λ) of 0.5 h, 0.35 h, and 0.2 h (h is the height of the cylindrical shell) and varying depth of the dimple of 1t, 2t, 3t, and 4t [3] (t is the thickness of the cylindrical shell). The FE models were generated using these imperfection patterns and they were numerically analysed using FE non-linear analysis including both material and geometrical non-linearities.

3   BUCKLING ANALYSIS

Types of buckling analysis are
   1. Eigen (or linear or bifurcation) buckling analysis
   2. Non-linear buckling analysis

3.1 Eigen buckling analysis

Eigen buckling analysis predicts the theoretical buckling strength of an ideal linear elastic structure. This analysis is used to predict the bifurcation point using linearised model of elastic structure. It is a technique used to determine buckling pressure-critical pressure-at which a structure becomes unstable and buckled mode shapes-the characteristic shape associated with a structure's buckled response. The other name for this eigen buckling analysis is "Bifurcation Analysis". The bifurcation buckling refers to unbounded growth of new deformation pattern. This analysis involves calculating the points at which the primary pressure deflection path is bifurcated by a secondary pressure deflection path. ANSYS finite element software package is used to determine the buckling strength of the perfect cylindrical shell through eigen buckling analysis. In eigen buckling analysis, imperfections and nonlinearities cannot be included. Sub-space iteration scheme can be used to extract the load factor or eigen value. The basic form of the eigen buckling analysis is given by

$$[K]\{\phi_i\} = \lambda_i [S]\{\phi_i\} \tag{1}$$

where

$[K]$ = Structural stiffness matrix
$\{\phi_i\}$ = Eigen vector
λ_i = Eigen value
$\{S\}$ = Stress stiffness matrix

3.2 Non-linear buckling analysis

This is a more accurate approach and since this FE analysis has capability of analyzing the actual structures with imperfections. This approach is highly recommended for design or evaluation of actual structures. This technique employs a non-linear structural analysis with gradually increasing loads to seek the pressure level at which the structure become unstable. Using this nonlinear technique, features such as initial imperfections, plastic behaviour etc., can be included in the model. In this analysis both geometrical and material nonlinearities are utilized, because the thin shell structures are subjected to large deformations and also at some of the imperfection location(s) on the structures the stresses may exceed elastic limit due to imperfections present in that location(s). Here the material non-linearity is defined with kinematic hardening rule. A full incremental nonlinear static stress analysis is used taking initial displacement (imperfections) matrix into account and applying pressure incrementally. In order to find the maximum load carrying capacity of the structure accurately, snap through approach of the non-linear analysis has to be followed. While using Newton-Raphson iteration scheme to solve system of equations in non-linear analysis near to the critical pressure of structure, the tangential stiffness matrix may become singular and thereby further pressure step is not possible. In order to overcome this problem, tangent iteration scheme is adopted.

4   FE MODELING

Eight noded quadrilateral shell elements, Shell93 of ANSYS are used for modeling the thin cylindrical shells. This element can handle membrane, bending and transverse shear effect, and also able to form curvilinear surface satisfactorily. This element also has plasticity, stress stiffening, large deflection and large strain capabilities.

4.1 Thin cylindrical shell model:

The thin cylindrical shell model taken for study [3] is:
Radius (r) = 1.9863m
Height (h) = 1.45m
Thickness (t) = 4.96mm
Poisson's ratio (p) = 0.3
Young's modulus (E) = 2.1 X 10^5 N/mm^2
Yield stress (σ_y) = 240 N/mm^2

     The same applied boundary condition given in Ref. [3] is also used in this work. Accordingly, the bottom edge is considered as fixed and the top edge is considered as ring stiffened and the external pressure load is applied on the external surface of the cylindrical shell models

4.2 FE model validation and mesh convergence study

To validate the FE results obtained, the eigen buckling pressure of perfect thin cylindrical shell under external pressure taken for the study is compared with the buckling pressure given in Ref. [3] with its first eigen mode shape. Table 1 shows the comparison of FE eigen buckling pressure obtained with the numerical solution given in Ref. [3]. Fig 1(a) and Fig 1(b) show the first eigen mode shape obtained from FE eigen bucking analysis in front and isometric view, respectively. From the mesh convergence study, the optimum number of elements for perfect cylindrical shell to predict the accurate solution is found to be 200×23 elements along circumferential and longitudinal directions. Thereby element selection and accuracy of the result are validated.

Table 1
Comparison of FE eigen buckling pressure with numerical results given in Ref. [3]

m	*n*	FE eigen buckling pressure result (KN/m²)	Numerical solution in [3] (KN/m²)	%Error
1	15	110.6	111.2	0.54

(a)   (b)

Fig. 1
FE first eigen buckling mode shape in (a): front view and (b): isometric view.

4.3 Modeling of imperfect cylindrical shells

It is well known that it is very difficult or sometimes even impossible to manufacture thin cylindrical shells without imperfections. Hence to obtain accurate result from numerical analysis is necessary to know about the exact shape and size of the imperfections which in turn depends on manufacturing process [18]. In most cases these data are not available. It is therefore generally recommended to have imperfection patterns like (i) first eigen mode shape, (ii) axisymmetric imperfection pattern namely inward half lobe imperfections pattern extended over the entire length of the cylindrical shell and (iii) local geometrical imperfections pattern namely inward dimple are chosen with the maximum amplitude of imperfections is varied depending upon the manufacturing processes. Hence in this work, for the first case the eigen vectors of the first eigen mode shape obtained from FE eigen buckling analysis is superimposed over the perfect cylindrical shell and for the other two cases the imperfections patterns are generated using mathematical Eq. (2) [3]. Before superimposing these imperfection patterns, at all the nodal point, these imperfection patterns are scaled so that the maximum amplitude (max amp) of imperfections is varied as 1*t*, 2*t*, 3*t*, and 4*t* to generate imperfect cylindrical shell models.

$$W_{amp} = \left(\frac{mh}{r} + n \right) t \tag{2}$$

The coefficients *m* and *n* are determined by

$$m = -5.6 \times 10^{-6} \left(\frac{r}{t} \right)^2 + 6.5 \times 10^{-3} \left(\frac{r}{t} \right) - 0.1$$

$$m = 1.3 \times 10^{-3} \left(\frac{r}{t} \right) - 0.4 \tag{2}$$

where W_{amp} is the maximum amplitude of imperfection, *h* is the height of the cylindrical shell, *r* is the radius of the cylindrical shell, and *t* is the thickness of the cylindrical shell. In the first and second cases, 200×23 elements are used along circumferential and longitudinal directions. In the third case, geometrical imperfections are local with change of curvature present in them may cause local bending stress [19]. In order to capture local bending stress, fine meshes used to the extent of 2 λ_b from the geometry of dimple is used for FE modeling.

$$\lambda_b = 1.732 \sqrt{rt} \tag{3}$$

5   RESULTS AND DISCUSSIONS

The FE models generated using the above said imperfection patterns are numerically analysed using FE non-linear analysis including both material and geometrical non-linearities.
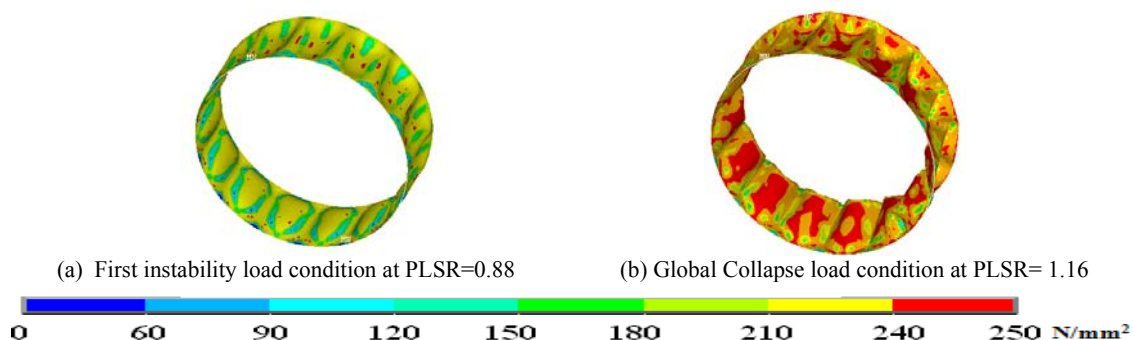
5.1 Eigen affine mode imperfection pattern

In this case, the eigen affine mode shape shown in Fig. 1 is superimposed on the FE model of perfect cylindrical shell to general imperfect shell models. Fig. 2 shows the snap through curves obtained from two diagonal nodal points whose coordinates are X= 1.97m, Y =0.12m, Z =0.75m and at X=-1.97m, Y =0.12m, Z =0.75m, respectively on the imperfect cylindrical shell model with maximum amplitude of imperfection ='3t'. Snap through curve is a curve obtained by plotting the Pressure Load Step Ratio (PLSR is defined as the ratio of the actual pressure applied at each load step to that of the eigen buckling pressure) and the nodal radial displacement. From these curves it can be observed that at the first instability point, at which the snap through curve as shown in Fig. 2 drops down first time with negative slope. On further loading, the slope of the snap through curve once again becomes positive and at collapse condition the cylindrical shell fails suddenly with large deformations. The PLSR at which the first instability point noticed is named as First Instability Buckling Pressure Ratio (FIBPR) and the PLSR at which the global collapse point noticed is named as Global Collapse Buckling Pressure Ratio (GCBPR). Fig 3(a) shows the von Mises stress contours of the cylindrical shell at first instability pressure condition when the maximum amplitude of imperfection is 3t. It can be noted that the maximum portion of the cylindrical shell reaches a stress condition just below the yield stress 240 N/mm^2 and only some parts of the cylindrical shell just crosses the yield stress value of 240 N/mm^2. Fig 3(b) shows the von Mises stress contours when the cylindrical shell reaches the collapse load condition. It can be noted from the Fig. 3(b) that at the collapse pressure point almost all portions of the cylindrical shell reaches the plastic condition.
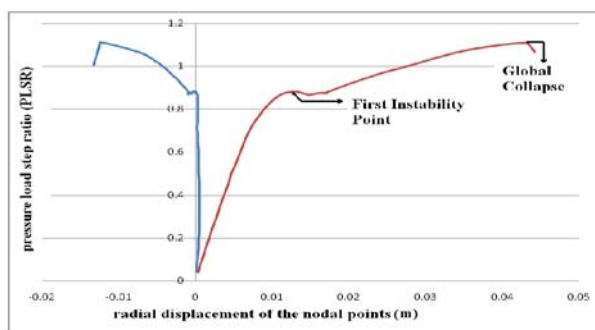
Fig. 2
Snap through curves taken at two diagonal nodal points on the imperfect cylindrical shell model with first eigen mode shape imperfection pattern having maximum amplitude of imperfections = 3t.

(a) First instability load condition at PLSR=0.88   (b) Global Collapse load condition at PLSR= 1.16

Fig. 3
Isometric views of von Mises stress contours of thin cylindrical shell model with first eigen mode shape imperfection pattern having maximum amplitude of imperfections = 3t; (a): at first instability load condition and (b): at global Collapse load condition (50 times enlarged).

Table 2 shows the variation of First Instability Point Buckling Pressure Ratio (FIBPR) and Global Collapse Point Buckling Pressure Ratio (GCBPR) for the variation in maximum amplitude of imperfections. It is observed that when compared to the lowest eigen buckling pressure (110600 N/m²) of the perfect cylindrical shell, FIBPR reduces by 11.5%, whereas GCBPR increases by 11.13% when the maximum amplitude of imperfections = 1*t*. When the maximum amplitude of imperfections increases from 1*t* to 4*t*, FIBPR reduces by 13.4% and GCBPR reduces by 6.23% when compared to the respective buckling pressure corresponding to 1*t*.
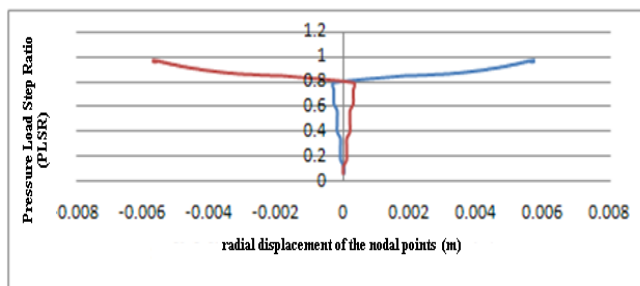
5.2 Inward half lobe axisymmetric imperfection pattern:

In this case, inward half lobe axisymmetric imperfection pattern is superimposed along the entire height of the FE perfect cylindrical shell model. Fig. 4 shows the snap through curves obtained from the same two nodal diagonal points at *X*= 1.97m, *Y* =0.12m, *Z* =0.75m and at *X*=-1.97m, *Y* =0.12m, *Z* =0.75m, respectively on the imperfect cylindrical shell model with maximum amplitude of imperfections = 3*t*.

Table 2
Imperfection ratio vs. FIBPR and GCBPR of imperfect cylindrical shell models with eigen affine imperfection pattern

Imperfection ratio (Wo/*t*)	First Instability Buckling Pressure Ratio (FIBPR)	Global Collapse Buckling Pressure Ratio (GCBPR)
1	0.885	1.1131
2	0.883	1.1108
3	0.88	1.1089
4	0.866	1.0508

Fig. 4
Snap through curves taken at two diagonal nodal points on the imperfect cylindrical shell model with inward half lobe axisymmetric imperfection pattern having maximum amplitude of imperfections = 3*t*.

(a) First instability load condition at PLSR=0.791   (b) Global Collapse condition at PLSR= 0.943
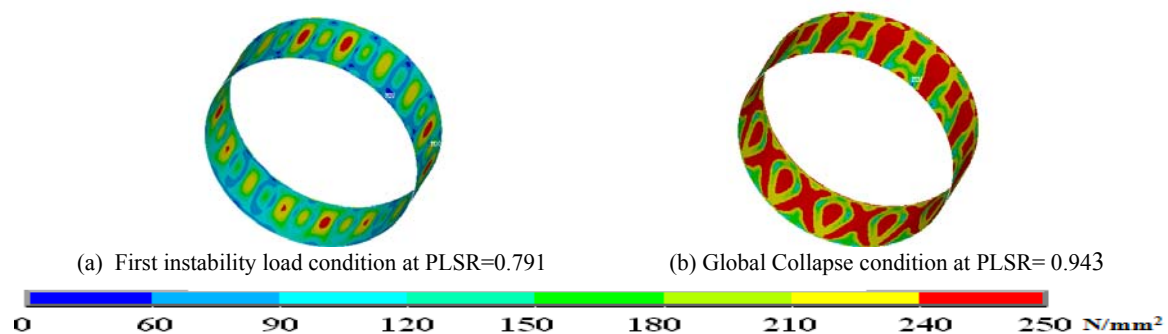
Fig. 5
Isometric views of von Mises stress contours of thin cylindrical shell model with inward half lobe axisymmetric imperfection pattern having maximum amplitude of imperfections = 3*t*; (a): at first instability load condition and (b): at global Collapse load condition (50 times enlarged).

Fig. 5(a) shows the von Mises stress contours at first instability point. It can be noted that here also the maximum portion of the cylindrical shell reaches a stress condition just below the yield stress 240 N/mm^2 and only in some portions of the cylindrical shell it just crosses the yield stress value of 240 N/mm^2. Fig 5(b) shows the von Mises stress contours when the cylindrical shell reaches collapse load condition and here also it can be noted almost all portions of the cylindrical shell reaches the plastic condition. Table 3 represents FIBPR and GCBPR values for increasing values of maximum amplitude of imperfections. Compared to that of the lowest eigen buckling pressure (110600 N/m^2) of the perfect cylindrical shell, FIBPR reduces by 5.8%, whereas GCBPR increases by 25.3% when the maximum amplitude of imperfections =1t. As the maximum amplitude of imperfections increases from 1t to 4t FIBPR reduces by 15.4% and GCBPR reduces by 34% when compared to the respective buckling pressures corresponding to 1t.

5.3 Single inward dimple imperfection pattern

Here, local imperfection pattern, namely single inward dimple imperfection pattern, is considered for $\lambda = 0.5\ h$, 0.35 h and 0.2 h, and depth varied as 1t, 2t, 3t, and 4t.

5.3.1 Single inward dimple with $\lambda=0.5\ h$

In this case, single inward dimple with $\lambda= 0.5\ h$ is superimposed at the mid height of the FE perfect cylindrical shell model. Fig. 6 represents snap through curve at the same two diagonal nodal points whose coordinates are $X= 1.97$m, $Y =0.12$m, $Z =0.75$m, and at $X=-1.97$m, $Y =0.12$m, $Z =0.75$m, respectively on the imperfect cylindrical shell model with maximum amplitude of imperfections=3t. Fig 7(a) shows the von Mises stress contours at first instability point. It can be noted that here also the maximum portion of the cylindrical shell reaches a stress condition just below the yield stress 240 N/mm^2 and only in some portions of the cylindrical shell it just crosses the yield stress value of 240 N/mm^2.

Fig 7(b) shows the von Mises stress contours when the cylindrical shell reaches collapse load condition. It can be noted from the Fig. 7(b) that at the collapse load condition almost all portions of the cylindrical shell reaches the plastic condition as in the case of eigen affine mode imperfection pattern.
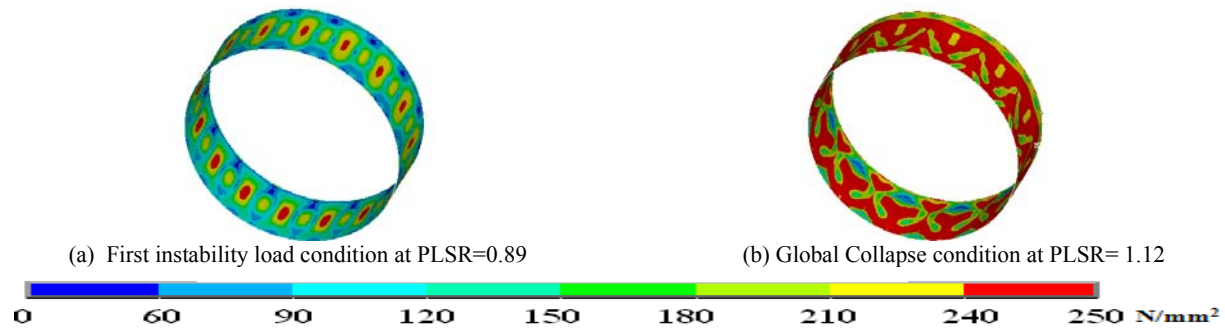
Table 3
Imperfection ratio vs. FIBPR and GCBPR of imperfect cylindrical shell models with inward half lobe axisymmetric imperfection pattern

Imperfection ratio (Wo/t)	FIBPR	GCBPR
1	0.942	1.253
2	0.878	0.978
3	0.791	0.943
4	0.788	0.913
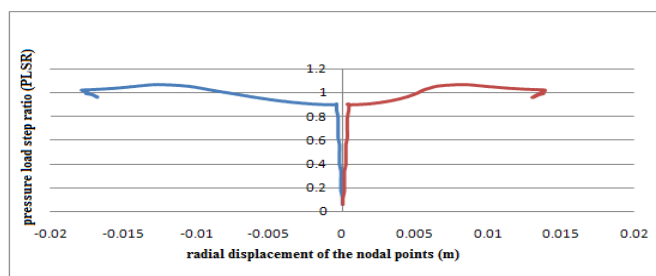
Fig. 6
Snap through curves taken at two diagonal nodal points on the imperfect cylindrical shell model with inward dimple imperfection pattern having $\lambda = 0.5\ h$ and maximum amplitude of imperfections = 3t.

(a) First instability load condition at PLSR=0.89   (b) Global Collapse condition at PLSR= 1.12

| 0 | 60 | 90 | 120 | 150 | 180 | 210 | 240 | 250 N/mm² |

Fig. 7
Isometric views of von Mises stress contours of thin cylindrical shell model with inward dimple imperfection pattern having λ = 0.5 h and maximum amplitude of imperfections = 3*t*; (a): at first instability load condition and (b): at global Collapse load condition (50 times enlarged).

Table 4
Imperfection ratio vs. FIBPR and GCBPR of imperfect cylindrical shell models with single inward dimple with λ=0.5 *h* imperfection pattern

Imperfection ratio (Wo/*t*)	FIBPR	GCBPR
1	0.921	1.49
2	0.903	1.32
3	0.89	1.12
4	0.845	0.97

Table 4 represents the variation of FIBPR and GCBPR values for increasing values of maximum amplitude of imperfections. When compared to the lowest eigen buckling pressure (110600 N/m²) of the perfect cylindrical shell, FIBPR reduces by 7.9%, where as GCBPR increases by 49% when the maximum amplitude of imperfections = 1*t*. As the maximum amplitude of imperfections increases from 1*t* to 4*t*, the FIBPR reduces by 15.5% and GCBPR reduces by 52% when compared to respective buckling pressures corresponding to 1*t*.

5.3.2 Single inward dimple with width 0.35 times the height of the cylindrical shell

In this case, single inward dimple as imperfection pattern with width 0.35 times the height of the cylindrical shell is superimposed along the mid-height of the FE perfect cylindrical shell. Table 5 represents FIBPR and GCBPR values for increasing values of maximum amplitude of imperfections. When compared to the lowest eigen buckling pressure (110600 N/m²) of the perfect cylindrical shell, FIBPR reduces by 1.9%, where as GCBPR increases by 54.5% when the maximum amplitude of imperfections = 1*t*. As the maximum amplitude of imperfections increases from 1*t* to 4*t*, FIBPR reduces by 10.9% and GCBPR reduces by 54% when compared to the respective buckling pressure corresponding to 1*t*.

5.3.3 Single inward dimple with λ=0.2 h

In this case, single inward dimple as imperfection pattern with width 0.20 times the height of the cylindrical shell is superimposed along the mid-height of the FE perfect cylindrical shell. Table 6 represents FIBPR and GCBPR values for increasing value of maximum amplitude of imperfections .When compared to the lowest eigen buckling pressure (110600 N/m²) of the perfect cylindrical shell, FIBPR reduces by 0.9%, whereas GCBPR increases by 93.3% when the maximum amplitude of imperfections = 1*t*. As the maximum amplitude of imperfections increases from 1*t* to 4*t*, FIBPR reduces by 12.6% and GCBPR reduces by 84.3% when compared to the respective buckling pressure corresponding to 1*t*.

Table 5
Imperfection ratio vs. FIBPR and GCBPR of imperfect cylindrical shell models with single inward dimple with λ=0.35 h imperfection pattern

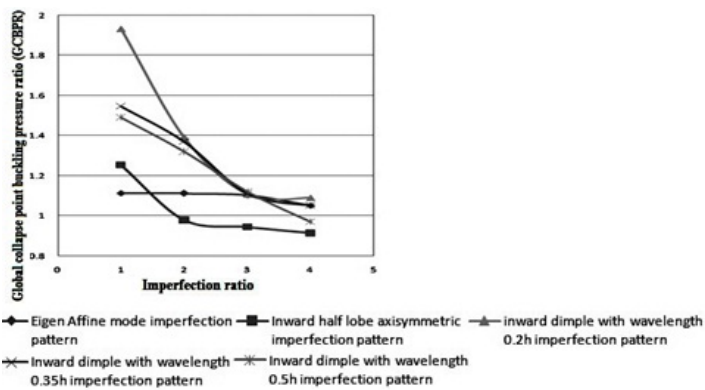| Imperfection ratio (Wo/t)	FIBPR	GCBPR
1	0.981	1.545
2	0.975	1.397
3	0.966	1.11
4	0.891	1.05

Table 6
Imperfection ratio vs. FIBPR and GCBPR of imperfect cylindrical shell models with single inward dimple with λ=0.2 h imperfection pattern

Imperfection ratio (Wo/t)	FIBPR	GCBPR
1	0.991	1.933
2	0.952	1.392
3	0.883	1.106
4	0.874	1.09
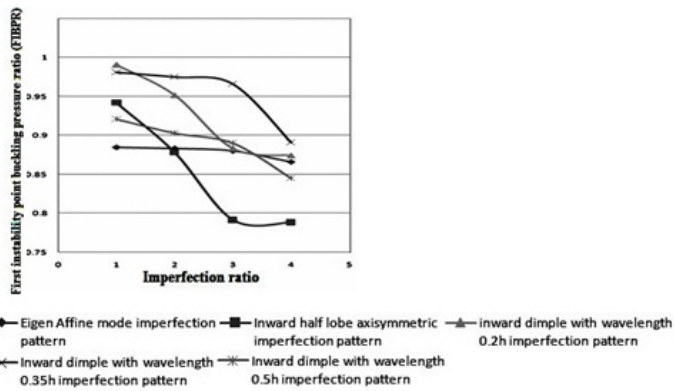
Fig. 8
Imperfection ratio vs. FIBPR curves of different imperfection patterns considered for study.

Fig. 9
Imperfection ratio vs. GCBPR curves of different imperfection patterns considered for study.

5.4 Comparative study of FIBPR and GCBPR for various imperfection patterns taken for study

Fig. 8 and Fig. 9 show the variation in FIBPR & GCBPR respectively for variation in amplitude of imperfections of the imperfection patterns considered for study. In the case of local dimple imperfection pattern, it is seen that as the wave length of imperfection increases, the buckling pressure decreases. From these graphs it can be observed that when the maximum amplitude of imperfections is 1t, the eigen affine imperfection pattern gives out the lowest FIBPR and GCBPR when compared to the other imperfection patterns considered. The amplitude of imperfections is above 1t, the inner half lobe axisymmetric imperfection pattern has the lowest FIBPR and GCBPR when compared to the other imperfection patterns.

6   CONCLUSION

The following conclusions are derived from the numerical analysis carried out on the thin cylindrical shell model with the different types of imperfection patterns taken for study.

I.   As the amplitude of imperfections increases the buckling pressure decreases.
II.   When the maximum amplitude of imperfections is 1t, the eigen affine imperfection pattern gives out the lowest FIBPR and GCBPR when compared to the other imperfection patterns considered and when the amplitude of imperfections is above 1t, the inner half lobe imperfection pattern gives out the lowest FIBPR and GCBPR when compared to the other imperfection patterns considered. i.e., local geometrical imperfections are not dominant compared to distribute geometrical imperfections in reducing the buckling pressure of cylindrical shell.
III.   When the maximum amplitude of imperfections increases, FIBPR decreases drastically in the case of inward half lobe axisymmetric imperfection pattern.
IV.   When the maximum amplitude of imperfections increases, GCBPR decreases drastically in the case of single Inward dimple with $\lambda = 0.2\ h$.
V.   In the case of local dimple imperfection pattern, it is seen that as the λ of the inward dimple increases, the buckling strength decreases.

7   ACKNOWLEDGEMENT

8   APPENDIX

1.	r	-	Radius of the Cylindrical Shell
2.	h	-	Height of the Cylindrical shell
3.	PLSR	-	Pressure Load Step Ratio
4.	FIBPR	-	First Instability Point Buckling Pressure Ratio
5.	GCBPR	-	Global Collapse Point Buckling Pressure Ratio
6.	$[K]$	-	Structural Stiffness Matrix
7.	$[S]$	-	Stress Stiffness Matrix
8.	t	-	Thickness of the Cylindrical Shell
9.	p	-	Poisson's Ratio
10.	n	-	No. of Lobes
11.	E_T	-	Tangential Young's Modulus
12.	λ_i	-	Eigen Value
13.	σ_v	-	Yield Stress
14.	$\{\varphi_i\}$	-	Eigen Vector
15.	λ	-	Wavelength of the dimple
16.	Wo	-	Maximum amplitude of imperfection

REFERENCES

[1]   Ross C.T.F., Little A.P.F., Adeniyi K.A., 2005, Plastic buckling of ring-stiffened conical shell under eternal hydrostatic pressure, *Ocean Engineering* **32**: 21-36.

[2]   Ross C.T.F., Little A.P.F., Allsop R., Smith, C., Engelhardt M., 2007, Plastic General instability of ring-reinforced conical shells under uniform external pressure, *Marine Technology* **44**(4): 268-277.

[3]   Schiender W., Brede A., 2005, Consistent equivalent geometric imperfections for the numerical buckling strength verification of cylindrical shells under uniform external pressure, *Thin-Walled Structures* **43**(2): 175-188.

[4]   Timoshenko P.S., Gere M.J., 1965, *Theory of Elastic Stability*, McGraw-Hill Publications, Second Edition, Singapore.

[5]   Brush D.O., Almroth B.O., 1975, *Buckling of Bars, Plates and Shells*, Chapter 5, McGraw-Hill, New York.

[6]   Bushnell D., 1985, *Computerized Buckling Analysis of Shells*, Martinus Nijhoff Publishers, Doedrecht.

[7]   Teng J.G., Song C.Y., 2001, Numerical models for nonlinear analysis of elastic shells with eigen mode-affine imperfections, *International Journal of Solids and Structures* **38**: 3263-3280.

[8]   Featherston C.A., 2003, Imperfection sensitivity of curved panels under combined compression and shear, *International Journal of Non-Linear Mechanics* **38**: 225-238.

[9]   Kim Seung-Eock, Kim Chang-Sung, 2002, Buckling strength of the cylindrical shell and tank subjected to axially compressive loads, *Thin-Walled Structures* **40**: 329-353.

[10]   Khelil, 2002, Buckling of steel shells subjected to non-uniform axial and pressure loadings, *Thin-Walled Structures* **40**: 955-970.

[11]   Pircher M., Berry P.A., Ding X., Bridge R.Q., 2001, The shape of circumferential weld-induced imperfections in thin-walled steel silos and tanks, *Thin-Walled Structures* **39**(12): 999-1014.

[12]   Koiter W.T., 2001, Elastic stability and post-buckling behaviour, *Journal of Structural Engineering* **127**(10): 1129-1136.

[13]   Khamlichi A., Bezzazi M., Limam A., 2004, Buckling of elastic cylindrical shells considering the effect of localized axisymmetric imperfections, *Thin-Walled Structures* **42**: 1035-1047.

[14]   Schiender W., 2006, Stimulating equivalent geometric imperfections for the numerical buckling strength verification of axially compressed cylindrical steel shells, *Comput. Mech.* **37**: 530-536.

[15]   Hutchinson J.W., Tennyson R.C., Muggeridge D.B., 1971, Effect of local axisymmetrical imperfection on the buckling behavior of a circular cylindrical shell under axial compression, *AIAA Journal* **9**: 48-52.

[16]   Amazigo J.C., Budiansky B., 1972, Asymptotic formulas for the buckling stresses of axially compressed cylinders with localized or random axisymmetric imperfections, *ASME Transactions*, *Journal of Applied Mechanics* **39**: 179-184.

[17]   Shen H.-S., Li Q.S., 2002, Thermo mechanical post buckling of shear deformable laminated cylindrical shells with local geometric imperfections, *International Journal of Solids and Structures* **39**: 4525-4542.

[18]   Song C.Y., Teng J.G., Rotter J.M., 2004, Imperfections sensitivity of thin elastic cylindrical shells subjected to axial compression, *International Journal of Solids and Structures* **41**: 7155-7180.

[19]   Arbocz J., Stranes J.H., 2004, On a verified high-fidelity analysis for axially compressed cylindrical shells, in: *45th AIAA/ASME/ASCE/AHS/ASC Structures, Structural Dynamics& Materials Conference*, 19-22 April 2004, Palm Springs, California, AIAA 2004-1712.

[20]   ANSYS 10 User Manual.